



CHORUS

This is the accepted manuscript made available via CHORUS. The article has been published as:

Spatial coherence in high-order-harmonic generation from periodic solid structures

Lu Liu, Jing Zhao, Wenpu Dong, Jinlei Liu, Yindong Huang, and Zengxiu Zhao

Phys. Rev. A **96**, 053403 — Published 7 November 2017

DOI: [10.1103/PhysRevA.96.053403](https://doi.org/10.1103/PhysRevA.96.053403)

Spatial coherence in high-harmonic generation from periodic solid structures

Lu Liu,¹ Jing Zhao,¹ Wenpu Dong,¹ Jinlei Liu,¹ Yindong Huang,¹ and Zengxiu Zhao ^{*1}

¹*Department of Physics, College of Science, National University of Defense Technology, Changsha 410073, Hunan, People's Republic of China*

We theoretically investigate the high-harmonic generation (HHG) from periodical structures driven by an intense laser pulse. Including the full bands, the single electron time-dependent Schrödinger equation (TDSE) is numerically solved in the velocity gauge using Bloch states to obtain the emission spectra. The contributions from different crystal sites are identified using the localized Wannier functions and time-frequency analysis. It is found that the cut-off energy of harmonics is depending on the migration distance of the electron and the instantaneous laser field strength when the electron transports into the related sites. We show that the coherence among different sites during electron propagation is crucial for HHG from solids which can be taken advantages to control the individual site contribution to the certain frequency range of the total harmonic spectra.

I. INTRODUCTION

High harmonic generation (HHG) from solids paves a new efficient way of producing ultra-short pulses into attosecond regime [1–9]. Subjected to long-wavelength strong few-cycle laser pulses, the optical and electronic properties of bulk crystalline solids are strongly modified transiently giving rise to various of non-perturbative characters [10]. In order to identify the physics behind, connection to and differentiation from the atomic gas cases are often being made with fruitful insights [6, 11], a complete understanding of HHG from solids is still being in pursuit.

For crystalline solids, the discrete bound states appearing in the atomic cases turn into bands of continuum with different crystal momenta. The energy-momentum dispersion relation deviates from the parabolic dispersion of atomic cases, which defines the scaling law of the cut-off harmonic energy for solids as a linear function of the driving laser field strength [1, 12, 13]. Within the mean-field approximation, the dynamics of HHG from a periodical structures can be understood in the single-electron picture. Following excitation from the valence band to the conduction band, the electron is driven under the laser field. When it recombines into the original hole state previously created in the valence band, harmonic is emitted with photon energy of the band gap at the corresponding instantaneous crystal momentum [12]. Such a generalized rescattering model for HHG from solids is thus proposed resembling the formulation of HHG from atomic gases [14–16]. Within this rescattering in two-band model, the cut-off energy cannot go beyond the maximum band gap. But clearly, when the laser intensity is high enough, the crystal momentum can go beyond the first Brillouin zone and higher bands come into play through Landau-Zener tunneling [17–21]. At the same time, multiple deflections of the electron wave at the edge

of the Brillouin zone causes the Bloch oscillations [22] of the induced electron current that emits harmonics with frequency in multiple integers of the Bloch frequency [5]. The complex dynamics involved stimulates the theoretical treatment of dividing the current into the intraband and the interband components [2] and full-band simulations [23–25] have recently been performed.

Because the crystalline solids are extended systems with periodic structures, the electron dynamics driven by the laser field and the resulted harmonic emission are encoded with spatial information [26, 27]. The coherent transport of the electron and the holes have significant effects on HHG. Due to the relaxation from inelastic scattering, the coherent length of the electron wave is limited which could hamper the harmonic emission. In addition, under the coherent excitation from strong laser fields, the dimension of electronic wave packet decreases and is confined into few crystal sites. The translational invariance of a periodic structure is destroyed resulting in the localized Wannier-Stark ladder states [28–30] with energy separated by the Bloch frequency Fa_0 , where a_0 is the lattice constant and F is the electric field strength. As hinted in our previous work [31] and others [32] on diatomic molecules with nuclear distance of R , the electron dynamics exhibits a drastic difference from the case of atoms that the ionized electron localized in one atomic core can migrate into the other core emitting harmonics at a cut-off energy of FR , which is analogy to the Bloch frequency. Therefore it would be interesting to investigate HHG from solids in the coordinate space and to explore how the coherence among electron waves localized at different sites contribute.

In this work, we calculate and analyze the harmonic spectra from a one-dimensional periodic structure subjected to a carrier-envelope phase (CEP) stabilized laser pulse. The time-dependent Schrödinger equation (TDSE) is solved in the basis of Bloch states [23, 33] in the velocity gauge, where the full bands are included. By examining the harmonic emission from each individual crystal site, we obtain the spatial information during the process of HHG. We identify that there exists quantum paths corresponding to the recombinations of the electron into crys-

*electronic mail: zhaozengxiu@nudt.edu.cn

tal sites different from the original site where the electron is localized initially. In particular, we show that the localized states are strongly dressed by the intense laser pulse, such that the maximum frequency of the harmonics is determined by the coherent propagation length and the dynamic Bloch frequency being proportional to the instantaneous laser field strength.

In order to mimic the decoherence effects, a spatial filter is applied in the simulation showing that the harmonic spectra is depending on how far the electron can be coherently transported. Such a coherence among different crystal sites is crucial for extending harmonic cut-off energy and for coherently manipulating HHG and other nonlinear processes such as high sideband generation [34, 35] in the presence of decoherence from electrons, phonons and defects. As a demonstration, we also show that the harmonic emission from different sites can be controlled by the CEP of the laser pulse, which can be used to better tailor the generated attosecond pulses.

This paper is organized as follows: In Sec. II, the method is summarized. In Sec. III, we present and discuss the numerical results of the harmonic emission spectra, with focus on the related electron dynamics and the effects of electron localization. A summary on the important finds is given in Sec. IV. Atomic units are used unless stated otherwise.

II. METHOD

Firstly we give a brief review of the methods for calculating HHG from a crystal lattice in laser fields (see, e.g., [23, 36]). The field-free eigenstates of the crystal electron can be found by solving the Schrödinger equation

$$\left[\frac{\mathbf{p}^2}{2m} + v(\mathbf{r}) \right] \phi_i^{\mathbf{k}} = \epsilon_i(\mathbf{k}) \phi_i^{\mathbf{k}}, \quad (1)$$

subjected to the periodical boundary condition, $\phi_i^{\mathbf{k}}(\mathbf{r} + \mathbf{L}) = \phi_i^{\mathbf{k}}(\mathbf{r})$, where m is the mass of the electron and \mathbf{L} corresponds to the size of the crystal which is macroscopically large. The periodical potential in the solid is given by $v(\mathbf{r})$ that $v(\mathbf{r} + \mathbf{a}_0) = v(\mathbf{r})$ with \mathbf{a}_0 being the lattice constant. According to the Bloch Theorem, the Bloch function takes the form of

$$\phi_i^{\mathbf{k}}(\mathbf{r}) = e^{i\mathbf{k}\cdot\mathbf{r}} u_i^{\mathbf{k}}(\mathbf{r}), \quad (2)$$

with $u_i^{\mathbf{k}}$ being a periodical function such that

$$u_i^{\mathbf{k}}(\mathbf{r} + \mathbf{a}_0) = u_i^{\mathbf{k}}(\mathbf{r}). \quad (3)$$

The eigenenergies $\epsilon_i(\mathbf{k})$ determine the dispersion relation between the electron energy and the crystal momentum \mathbf{k} within the i^{th} band.

Subjected to an external time-varying electro-magnetic field represented by the vector potential $\mathbf{A}(t)$, the time evolution of the crystal can be described by the time-

dependent Schrödinger equation (TDSE) in the velocity gauge

$$i \frac{\partial}{\partial t} \psi^{\mathbf{k}}(t) = \left[\frac{[\mathbf{p} - e\mathbf{A}(t)]^2}{2m} + v(\mathbf{r}) \right] \psi^{\mathbf{k}}(t), \quad (4)$$

where $e = -1$ is the electron charge in atomic units and the dipole approximation has been assumed. The total wave function is expanded by using the unperturbed Bloch functions,

$$\psi^{\mathbf{k}}(t) = \sum_i a_i^{\mathbf{k}}(t) \phi_i^{\mathbf{k}}, \quad (5)$$

where i runs over the accessible bands. We explicitly label the wave function by \mathbf{k} that is conserved when neglecting the inelastic scattering by electrons and phonons.

Assuming all the electron initially occupying in the highest valence band with every particular crystal momentum \mathbf{k} , the current density driven by the laser field can be expressed by

$$\mathbf{j}_n^{\mathbf{k}}(t) = \frac{e}{m} \left(\langle \psi_n^{\mathbf{k}}(t) | \mathbf{p} | \psi_n^{\mathbf{k}}(t) \rangle - e\mathbf{A}(t) \right). \quad (6)$$

The time-dependent laser-induced macroscopic current $\mathbf{j}(t)$ is given by:

$$\mathbf{j}(t) = \sum_n \int \mathbf{j}_n^{\mathbf{k}}(t) d^3\mathbf{k}. \quad (7)$$

The harmonic spectra can be obtained by the Fourier transformation of the macroscopic current.

In the numerical implementation, the Bloch functions are expanded using a set of N_{max} plane waves,

$$u_i^{\mathbf{k}}(\mathbf{r}) = \sum_{j=1}^{N_{max}} C_{i,j}^{\mathbf{k}} \exp[i\mathbf{K}_j \cdot \mathbf{r}], \quad (8)$$

where $\mathbf{K}_j = \sum_{\alpha=1}^3 m_j^\alpha \mathbf{b}_\alpha$ denote reciprocal lattice vectors, m_j^α are integers and \mathbf{b}_α are the primitive vectors of the reciprocal lattice. The periodical potential $v(\mathbf{r})$ can be represented in the basis of Fourier series:

$$v(\mathbf{r}) = \sum_{j=1}^{N_{max}} v_j e^{i\mathbf{K}_j \cdot \mathbf{r}}, \quad (9)$$

with

$$v_j = \frac{1}{\Omega} \int_{\Omega} e^{-i\mathbf{K}_j \cdot \mathbf{r}} v(\mathbf{r}) d\mathbf{r}, \quad (10)$$

where Ω is the volume of a site.

Alternatively, the TDSE can be solved directly on the grids in the coordinate space. Both methods has been applied in this investigation and agreement has been reached. The space coordinate representation helps to

connect the understanding of HHG from crystals and from atoms. For example, we can identify the spatial information of HHG processes by constructing the Wannier function [29] from i^{th} band localized at the n^{th} site through

$$\psi_i^{\mathbf{R}}(\mathbf{r}) = \sum_{\mathbf{k}} e^{-i\mathbf{k}\cdot\mathbf{R}} \phi_i^{\mathbf{k}}(\mathbf{r}), \quad (11)$$

where $\mathbf{R} = n\mathbf{a}_0$. The individual contribution to HHG from the n^{th} site can be obtained by projecting the time-dependent wave function to the Wannier state localized at \mathbf{R} :

$$\mathbf{j}_i^{\mathbf{R}}(t) = \text{Re} \left[\left\langle \sum_{\mathbf{k}} \psi^{\mathbf{k}} | \mathbf{p} - e\mathbf{A} | \psi_i^{\mathbf{R}} \right\rangle \left\langle \psi_i^{\mathbf{R}} | \sum_{\mathbf{k}} \psi^{\mathbf{k}} \right\rangle \right] \quad (12)$$

The single active electron approximation is applied in the formulation above, which suffers from neglecting the decoherence from the inelastic scattering by lattices and electrons. It can be partially remedied by incorporating an imaginary potential $U_{\Gamma}(\mathbf{r})$ into the field-free hamiltonian

$$\hat{H}_0 = -\frac{\hbar^2}{2m} \nabla^2 + v(\mathbf{r}) - iU_{\Gamma}(\mathbf{r}). \quad (13)$$

In such a treatment, the eigenenergies become complex values $\epsilon_i(\mathbf{k}) - i\frac{\Gamma}{2}$, where $T = \frac{1}{\Gamma}$ gives the relaxation time. On the other hand, $U_{\Gamma}(\mathbf{r})$ can also serve as a spatial filter by proper choices to suppress those contributions from far reached crystal sites when solving the TDSE in the coordinate space. It helps identifying the individual contributions from different sites to HHG as shown later.

III. RESULTS AND DISCUSSIONS

A. The dynamics of HHG in association with electronic trajectory in x-space based on numerical solving of TDSE

In Fig.1, we present the harmonic spectra calculated from solving the single electron TDSE in one-dimension with a periodical pseudo potential, $V(x) = -0.37[1 + \cos(2\pi x/a_0)]$, where the lattice constant $a_0 = 8 \text{ a.u.}$. The highest valence band and the lowest four conduction bands are shown in Fig. 1(a). The single cycle laser pulse has a Gaussian profile with the center wavelength of $3.2 \mu\text{m}$, and the intensity of $5\text{TW}/\text{cm}^2$. The highest VB are fully populated at the initial time.

Once the time-dependent Bloch wave functions are found, the harmonic spectrum is obtained by the Fourier transformation of the macroscopic current in Eq. 7, which is shown in Fig. 1(b) with **black solid line**. Three obvious plateaus are visible whose energies correspond to the band gap energies between the highest VB and the second CB (1.06 a.u.), the third CB (1.75 a.u.) and the fourth CB (2.51 a.u.), indicated by the vertical dotted

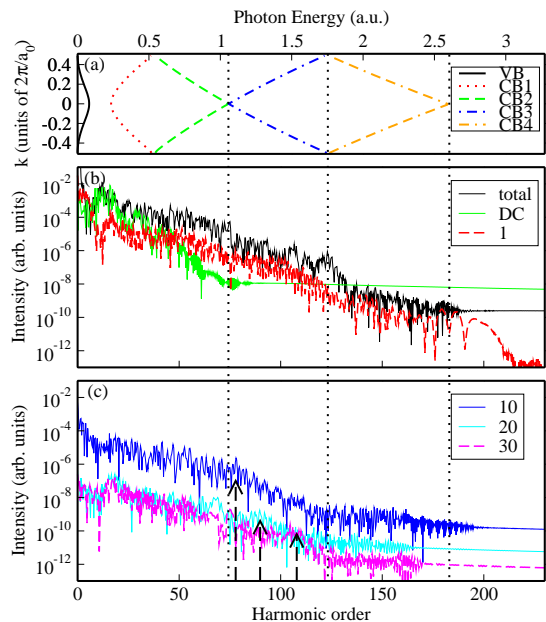


FIG. 1: (a) The band structure used in our calculation, which contains the highest VB and the four CBs. (b) The total harmonic spectrum is plotted with black solid line. The black dotted lines mark three obvious plateaus of the total harmonics, which corresponding to the bandgaps among the highest VB and the high-lying CBs. The green (grey) line represents the decoherent summation (DC) of current under the action of a spatial filter with width is $10a_0$. The separated harmonic spectra from Wannier state localized at 1^{th} crystal site is shown with red dashed line. (c) The separated harmonic spectra from Wannier states localized at 10^{th} , 20^{th} and 30^{th} crystal sites are shown with solid blue line, cyan (grey) line and dashed magenta line respectively. The black dashed arrows mark the cut-off of the harmonic spectra.

black lines [24].

The information of the band structure can be deduced from the harmonic spectrum, while the dynamics of the electrons in solids are closely related to the spatial periodic structure. We use a spatial filter whose width is $10a_0$ to mimic the decoherence effects in simulation. The decoherent current induced harmonic spectrum is shown with **green (grey) line**, while the cutoff energy of the decoherent harmonic is significantly suppressed by the coherent distance $10a_0$. This means that the harmonic spectrum is depending on the spatial distance of the electron can coherently transport. In order to investigate the spatial structure dependence of the HHG from solids, the Bloch wave function of the highest VB is converted to the Wannier wave functions localized at different R using Eq. 11. The total time-dependent wave function can be projected on the localized Wannier states in different crystal sites of the highest VB, which is used to separate the contributions of different sites to the total high harmonics. In the coordinate space calculation, the size of box is from $-100a_0$ to $100a_0$. The harmonic spectra emitted from certain crystal sites located at a_0 , $10a_0$, $20a_0$, $30a_0$ are

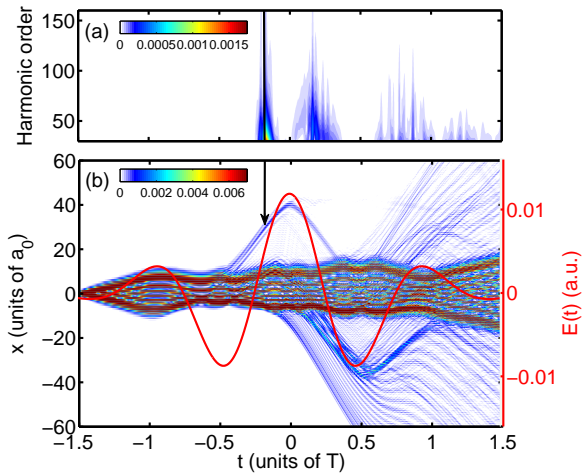


FIG. 2: (a) The time-frequency analysis of the separated harmonics from 30^{th} site is shown. (b) The trajectories of electrons in coordinate space and the corresponding time-dependent electric field (red solid line) are shown. The black arrow indicates the moment t_r^{30} of the electron transitioning to 30^{th} site.

shown in Fig. 1(b) and (c) with the dashed red line, solid blue line, cyan (grey) line and dashed magenta line respectively. The separated harmonic spectra from the crystal sites located at a_0 , $10a_0$ have nearly no obvious difference from the total spectrum, except for the overall variation of harmonic intensities.

On the other hand, the harmonic spectra generated from crystal sites beyond $10a_0$ show an extension of harmonic order as indicated by the vertical black dashed arrows in Fig. 1(c). In order to understand the difference, we shown in Fig. 2 (b) the time evolution of the electron density in coordinate space. It is found that the initially localized electronic wave function (at site 0) spreads quickly into the neighboring 10 sites due to the quantum diffusion caused by the valence band dispersion. Because of this delocalization, it is hard to differentiate the individual site contribution from the harmonic spectra generated from the first 10 sites. However, as the laser field continues to grow, the electron starts to move beyond the first 10 sites. As shown in Fig. 2 (b), the electron can be found even beyond $50a_0$. We are going to show below that the extension of harmonic cut-off is related to the electron localization in far reached sites.

In Fig. 2(a), we show the time-frequency analysis [12] of the harmonics generated from the Wannier state localized at 30^{th} crystal site. It can be seen there exists that two major emission instants at $t_1 = -0.16T$ and $t_2 = 0.14T$, also there is a weaker harmonic emission after $t_3 = 0.7T$. The three instants corresponds exactly to the moments that the electron pass through the site at $30a_0$ as indicated by the black arrow for the earlier one in Fig. 2(b). The connection demonstrates that HHG from site 30 occurs at the instant that the electron recombines into the site 30. But what determines the maximum en-

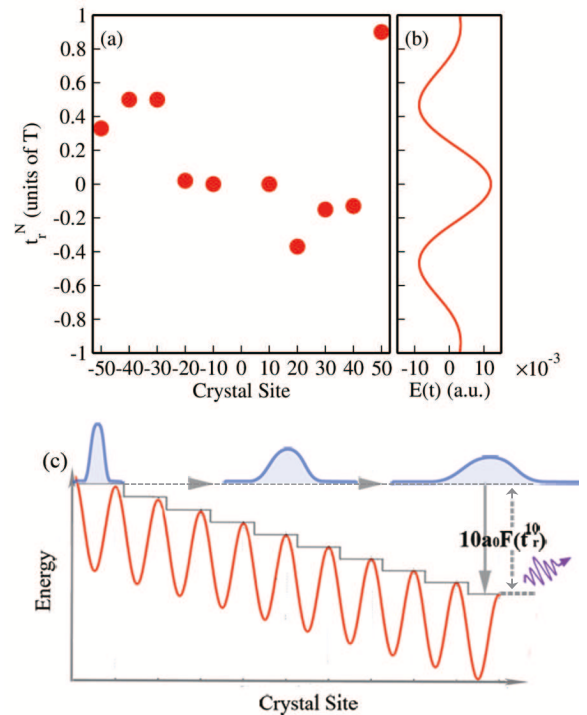


FIG. 3: (a) The red dots represent the moments of electrons transitioning to Wannier state localized at $-50a_0$, $-40a_0$, $-30a_0$, $-20a_0$, $-10a_0$, $10a_0$, $20a_0$, $30a_0$, $40a_0$, $50a_0$ respectively, which contribute to the cut-off energies of the separated harmonics. (b) The corresponding laser field. (c) Schematic illustration of the electron transitioning from the central site to the 10^{th} site in the field-driven potential wells, which arrange like a ladder.

ergy of the emitted harmonics?

We denote the moment t_1 when the electrons transit to 30^{th} site as t_r^{30} . It can be seen that the harmonic emitted at this instant is much higher than those emitted after $t_3 = 0.7T$. It suggests that not only the distance of the electron migrating in the real space matters, but also the corresponding instantaneous laser field strength is crucial. The moments t_r^N when the electron transits to $N = -50, -40, -30, -20, -10, 10, 20, 30, 40, 50$ site are shown in Fig. 3(a) with red dots which are deduced from both the electronic trajectories and the time-frequency analysis. The corresponding electric field strength $F(t_r^N)$ can be found from Fig. 3(b) that depicts the electric profile of the applied laser field. For example, the instantaneous field strength of the electrons move to the 30^{th} site $F(t_r^{30})$ are equal $0.0062 a.u.$. It is surprising to find that the harmonic cut-off energy, calculated from the spectra using the localized Wannier function and the time-frequency analysis, both equals to $30a_0F(t_r^{30})$.

In connection to our previous investigations about the harmonic energies released from molecules [31], we here propose a mechanism of HHG from periodical structures in real space. For HHG from diatomic molecules, we have demonstrated that the electron localized in one of the

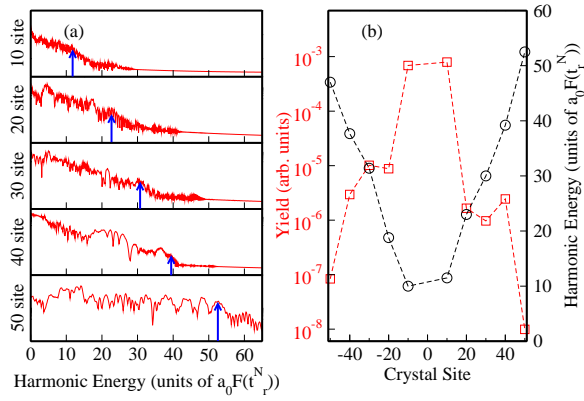


FIG. 4: (a) The separated harmonic spectra from Wannier states localized at different crystal sites are shown. The blue arrows indicate the cut-off energies. (b) The cut-off energies of high harmonics from the Wannier states localized at different crystal sites are shown with black circles. The corresponding harmonic yields are labelled with red squares.

potential wells can recombine not only with the original well, but also with the other one in different trajectories and release different harmonic energies. One possible trajectory is that electrons migrate between the laser field dressed potential wells, which contributes to harmonics with the energy FR , i.e. the energy difference between the two laser dressed wells where R is the internuclear distance. Analogously, HHG from solids exhibits similar picture. For the carriers in the periodic potential subjected to an intense electric field applied in the x direction, Wannier-Stark Ladder states are formed [30] and the resulting eigenspectrum is discrete and equidistant, scaling linearly with the electric field strength. The energy difference between neighboring states is Fa_0 , and the strong field dressed localized electronic wavefunction has a long tail of the exponential decay spreading through several crystal sites. Therefore when the electrons recombine into the N -th site, the radiated harmonic energy is NFa_0 as illustrated in Fig. 3(c). Based on this mechanism we proposed, the cut-off energies of harmonics from localized Wannier function at N^{th} crystal site can be evaluated by $Na_0F(t_r^N)$.

In order to verify this model, we replot the harmonic spectra generated from N^{th} crystal site with energy in units of $a_0F(t_r^N)$ shown in Fig. 4(a). It can be seen clearly that as the crystal sites are further away from the origin, the harmonic cut-off (indicated by the blue arrows) is increased (from $10a_0$, $20a_0$, $30a_0$, $40a_0$ to $50a_0$). To better demonstrating the dependence, the cut-off energies of harmonics from the different crystal sites are shown with black circle in Fig. 4 (b). It is found that the cut-off is directly proportional to the distance of the localized Wannier state from the origin, in agreement with our expectation. We also show the harmonic yields from different sites by integrating the harmonics at the plateau in Fig. 4 (b). The yields decrease when the Wannier state is localized at further crystal site. It is consistent

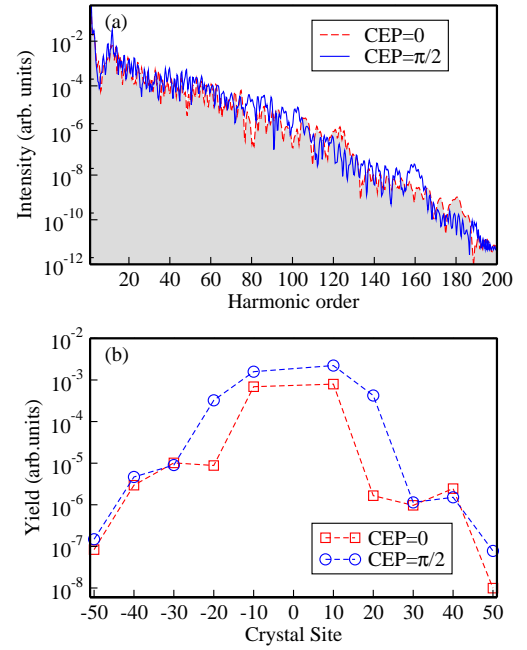


FIG. 5: (a) The high harmonics spectra from the laser fields with CEP=0 and CEP= $\pi/2$ are showed with red dashed line and blue solid line, respectively. (b) The harmonic yields from different crystal sites under the laser fields with CEP=0 and CEP= $\pi/2$ are shown with red squares and blue circles, respectively.

with the actual situation of electrons in periodic structure that fewer electrons move to longer distance due to the dispersion. In addition, we expect that the contribution from sites far away from the origin will be weakened further under the action of decoherence and scattering between electrons and lattices.

The trajectories of electrons in periodic structure is sensitively dependent on the carrier-envelope phase (CEP) of the few-cycle laser field. The harmonic spectra therefore reflects the spatial dynamics of electrons. As shown in Fig. 5(a), the total harmonic spectra for the laser fields with CEP=0 and CEP= $\pi/2$ are compared. The two spectra are similar below 70^{th} harmonic order, while the intensity of harmonics generated from the laser field with CEP= $\pi/2$ shows an obvious enhancement from 70^{th} to 100^{th} order compared to the spectra with CEP=0. The individual harmonic yields from different crystal sites are compared in Fig. 5(b) for two CEPs. Because there is no significant difference between the harmonic yields from the 10^{th} site (-10^{th} site) with different CEP, the harmonics below 70^{th} order mainly contributed from the 10 sites are almost the same. Nevertheless, the harmonic yield of 20^{th} site (-20^{th} site) from CEP= $\pi/2$ is increased by about two orders of magnitude compared with CEP=0. This is clearly reflected in the area from 70^{th} to 100^{th} order of the harmonic spectrum, which is just the contribution of the 20^{th} site. Therefore, it is possible to observe and control the contributions from different crystal sites by adjusting the CEP of laser field in experiments. These

investigations are helpful to guide the future experimental study about the electronic dynamics in solids.

IV. SUMMARY

In conclusion, the dynamics of electrons are investigated through numerically solving the TDSE in the Bloch basis. Based on the delocalized Bloch function in momentum space, the total high harmonic spectrum shows several plateaus, and the band structure information can be deduced. In addition, it is more intuitionistic to conceptualize the dynamics of electrons in real space. The calculated trajectories in real space show that the initially localized electrons can transit far away in the crystal sites arranged like a ladder under the strong laser

field, during which the electrons show the significant localization. The separated contribution in total harmonics from a single crystal site is calculated by the localized Wannier function to investigate the localization. We find out that the separated harmonic energy is proportional to both the distance the electrons migrate and the instantaneous field strength. Because of the obvious CEP dependence of the trajectories, our work paves the way to control the localized contributions from a certain crystal site to HHG from solid. It is valuable to synthesize the attosecond pulse and probe the complicated periodic structure and the electron dynamics of the solid on a micrometer scale. This work is supported by the National Basic Research Program of China (973 Program) under Grant No.2013CB922203, and the NSF of China (Grant No.11374366 and No.11404401).

-
- [1] S. Ghimire, A. D. DiChiara, E. Sistrunk, P. Agostini, L. F. DiMauro, and D. A. Reis, *Nature Physics* **7**, 138 (2010).
- [2] G. Vampa, C. R. McDonald, G. Orlando, D. D. Klug, P. B. Corkum, and T. Brabec, *Phys. Rev. Lett.* **113**, 073901 (2014).
- [3] O. Schubert, M. Hohenleutner, F. Langer, and B. Urbanek, *Nature Photonics* **8**, 119 (2014).
- [4] M. Hohenleutner, F. Langer, O. Schubert, M. Knorr, U. Huttner, S. W. Koch, M. Kira, and R. Huber, *Nature* **523**, 572 (2015).
- [5] T. T. Luu, M. Garg, S. Y. Kruchinin, A. Moulet, M. T. Hassan, and E. Goulielmakis, *Nature* **521**, 498 (2015).
- [6] G. Ndabashimiye, S. Ghimire, M. Wu, D. A. Browne, K. J. Schafer, M. B. Gaarde, and D. A. Reis, *Nature* **534**, 520 (2016).
- [7] T. Tamaya, A. Ishikawa, T. Ogawa, and K. Tanaka, *Phys. Rev. Lett.* **116**, 016601 (2016).
- [8] T. Meier, G. von Plessen, P. Thomas, and S. W. Koch, *Phys. Rev. Lett.* **73**, 902 (1994).
- [9] D. Golde, T. Meier, and S. W. Koch, *J. Opt. Soc. Am. B* **23**, 2559 (2006).
- [10] M. Lucchini, S. A. Sato, A. Ludwig, J. Herrmann, M. Volkov, L. Kasmir, Y. Shinohara, K. Yabana, L. Gallmann, and U. Keller, *Science* **353**, 916 (2016).
- [11] G. Vampa, B. G. Ghamsari, S. Siadat Mousavi, T. J. Hammond, A. Olivieri, E. Lisicka-Skrek, A. Y. Naumov, D. M. Villeneuve, A. Staudte, P. Berini, et al., *Nature physics* **64**, 39 (2017).
- [12] G. Vampa, C. R. McDonald, G. Orlando, P. B. Corkum, and T. Brabec, *Phys. Rev. B* **91**, 064302 (2015).
- [13] Z. Guan, X. Zhou, and X. Bian, *Phys. Rev. A* **93**, 033852 (2016).
- [14] P. B. Corkum, *Phys. Rev. Lett.* **71**, 1994 (1994).
- [15] M. Lewenstein, P. Balcou, Y. M. Ivanov, A. LHuillier, and P. B. Corkum, *Phys. Rev. A* **49**, 2117 (1994).
- [16] J. Zhao and Z. Zhao, *Phys. Rev. A* **78**, 1 (2008).
- [17] C. Zener, *Proceedings of the Royal Society of London A: Mathematical, Physical and Engineering Sciences* **145**, 523 (1934).
- [18] D. Golde, T. Meier, and S. W. Koch, *Phys. Rev. B* **77**, 075330 (2008).
- [19] D. Golde, M. Kira, T. Meier, and S. W. Koch, *Physica Status Solidi (B)* **248**, 863 (2010).
- [20] C. R. McDonald, G. Vampa, P. B. Corkum, and T. Brabec, *Phys. Rev. A* **92**, 033845 (2015).
- [21] C. Yu, X. Zhang, S. Jiang, X. Cao, G. Yuan, T. Wu, L. Bai, and R. Lu, *Phys. Rev. A* **94**, 013846 (2016).
- [22] F. Bloch, *Zeitschrift für Physik* **52**, 555 (1929).
- [23] M. Korbman, S. Y. Kruchinin, and V. S. Yakovlev, *New J. Phys.* **15**, 013006 (2013).
- [24] M. Wu, S. Ghimire, D. A. Reis, K. J. Schafer, and M. B. Gaarde, *Phys. Rev. A* **91**, 043839 (2015).
- [25] N. Tancogne-Dejean, O. D. Mücke, F. X. Kärtner, and A. Rubio, *Phys. Rev. Lett.* **118**, 087403 (2017).
- [26] Y. S. You, D. A. Reis, and S. Ghimire, *Nature physics* **13**, 345 (2017).
- [27] E. N. Osika, A. Chacón, L. Ortmann, N. Suárez, J. A. Pérez-Hernández, B. Szafran, M. F. Ciappina, F. Sols, A. S. Landsman, and M. Lewenstein, *Phys. Rev. X* **7**, 021017 (2017).
- [28] H. Wannier, G. *Elements of Solid State Theory* (Cambridge U. P., Cambridge, England, 1959).
- [29] G. H. Wannier, *Phys. Rev.* **117**, 432 (1960).
- [30] E. E. Mendez and G. Bastard, *Physics Today* **46**, 34 (1993).
- [31] L. Liu, J. Zhao, J. Yuan, and Z. Zhao, *SCIEN-TIA SINICA Physica, Mechanica and Astronomica* **47**, 033006 (2017).
- [32] X. B. Bian and A. D. Bandrauk, *Phys. Rev. Lett.* **105**, 093903 (2010).
- [33] J. B. Krieger and G. J. Iafrate, *Phys. Rev. B* **33**, 5494 (1986).
- [34] B. Zaks, R. B. Liu, and M. S. Sherwin, *Nature* **483**, 580 (2013).
- [35] J. A. Crosse, X. Xu, M. S. Sherwin, and R. B. Liu, *Nature Communications* **5**, 4854 (2015).
- [36] H. Bachau, A. N. Belsky, P. Martin, A. N. Vasilev, and B. N. Yatsenko, *Phys. Rev. B* **74**, 235215 (2006).